Photodiagnosis and Photodynamic Therapy 26 (2019) 101–110

Contents lists available at ScienceDirect

Photodiagnosis and Photodynamic Therapy

journal homepage: www.elsevier.com/locate/pdpdt

Photophysical properties and photodynamic therapy activities of detonated nanodiamonds-BODIPY-phthalocyanines nanoassemblies

Refilwe Matshitse, Bokolombe P. Ngoy, Muthumuni Managa, John Mack, Tebello Nyokong*

Centre for Nanotechnology Innovation, Department of Chemistry, Rhodes University, South Africa

ARTICLE INFO

Keywords:
Detonated nanodiamonds
Pyridyloxy
Zinc phthalocyanine
Photodynamic therapy
BODIPY

ABSTRACT

This work reports on the synthesis of nanoassemblies of supramolecular hybrids containing detonated nanodiamonds (DNDs) covalently linked to halogenated BODIPY (DNDs-BODIPY) by an amide bond, followed by π–π stacking of 2,9,16,23-tetrakis[4-(*N*-methylpyridyloxy)]-phthalocyanine (ZnTPPcQ) on the DNDs-BODIPY conjugate, to form nanoassembly represented as ZnTPPcQ-DNDs-BODIPY. ZnTPPcQ-DNDs-BODIPY has a higher singlet oxygen quantum yield of 0.50 in water. Therefore, the construction of a three component photodynamic therapy agent (ZnTPPcQ-DNDs-BODIPY) as a single photosentisiser improved singlet quantum yields of the Pc. Zeta potential studies of ZnTPPcQ-DNDs-BODIPY under various temperatures, concentrations and pH conditions, showed the conjugate is more stable at pHs 2, 4 and 7 and at high concentrations (50 μg/mL) and temperatures (80 °C). ZnTPPcQ-DNDs-BODIPY showed high photodynamic therapy (PDT) activity with a low MCF-7 cell viability of 21 ± 5% when compared to 31 ± 2%, 30 ± 2% and 28 ± 2% cell viability at the highest tested concentration of 50 μg/mL for DNDs, ZnTPPcQ-DND and DNDs-BODIPY, respectively.

1. Introduction

Metallophthalocyanines (MPcs) have gained interest for applications in a number of areas including: imaging, nonlinear optics, photodynamic antimicrobial chemotherapy (PACT) and photodynamic therapy (PDT) because of their excellent physical and chemical properties [1–4]. Interest in MPcs as potential PDT agents could be attributed to several factors such as their ability to absorb in the near infrared region of the electromagnetic spectrum (allowing for deep tissue penetration) and to efficiently generate singlet oxygen and other reactive oxygen species (ROS) that can destroy cancer cells and pathogenic microbes [5–7].

On the other hand, research on borondipyrromethenes (BODIPYs) dyes as potential photosentisisers for PDT is on the increase [8,9]. BODIPYs exhibit ideal photosensitiser characteristics including resistance to photobleaching and high light–dark toxicity ratios [10]. BODIPYs have been extensively studied as fluorescence imaging probes when compared to PDT since they are highly fluorescent reducing intersystem crossing to the triplet state [10,11]. Consequently, BODIPYs for use in PDT have to be modified to depress fluorescence and enhance singlet-to-triplet intersystem crossing. Improved singlet oxygen generation properties of halogenated styryl-substituted BODIPY have been previously reported [10]. Hence, halogenated BODIPY dyes are used in this study. Hybrids of BODIPYs with phthalocyanines are very few, and have been shown to have high singlet oxygen quantum yields [11–14]. The current work reports for the first time on the PDT activity of hybrids containing a Pc and BODIPY. The reported [15] 3,5-di-*p*-benzyloxystyryl BODIPY was employed due to the red-shifted spectra, which is essential for PDT.

Recently our group reported on a hybrid structure containing BODIPY, MPc and graphene quantum dots (GQDs) [14]. The current work reports on a composite containing BODIPY, positively charged MPc and detonated nanodiamond (DNDs) as a platform for potential use in PDT. In their pristine state, DNDs contain several functional groups on the surface including amine, amide, alcohol, carbonyl, and carboxyl [16–20]. Some of these are not present in pristine GQDs, hence the two nanomaterials are expected to influence the photophysical and PDT activities of the photosensitisers differently. The functional groups on DNDs facilitate the linking of DNDs to other molecules such as BODIPYs and Pcs.

In this work, we construct a nanocomposite consisting of MPc (positively charged), BODIPY and DNDs with the aim of improving PDT activity through synergistic effect. A positively charged MPc is employed since a comprehensive analysis of twenty-two cancer cell lines taken from different body parts showed that all the cells specifically bound to positively charged nanoprobes, suggesting that cancer cells

* Corresponding author.
E-mail address: t.nyokong@ru.ac.za (T. Nyokong).

https://doi.org/10.1016/j.pdpdt.2019.03.007
Received 6 January 2019; Received in revised form 13 February 2019; Accepted 4 March 2019
Available online 06 March 2019
1572-1000/

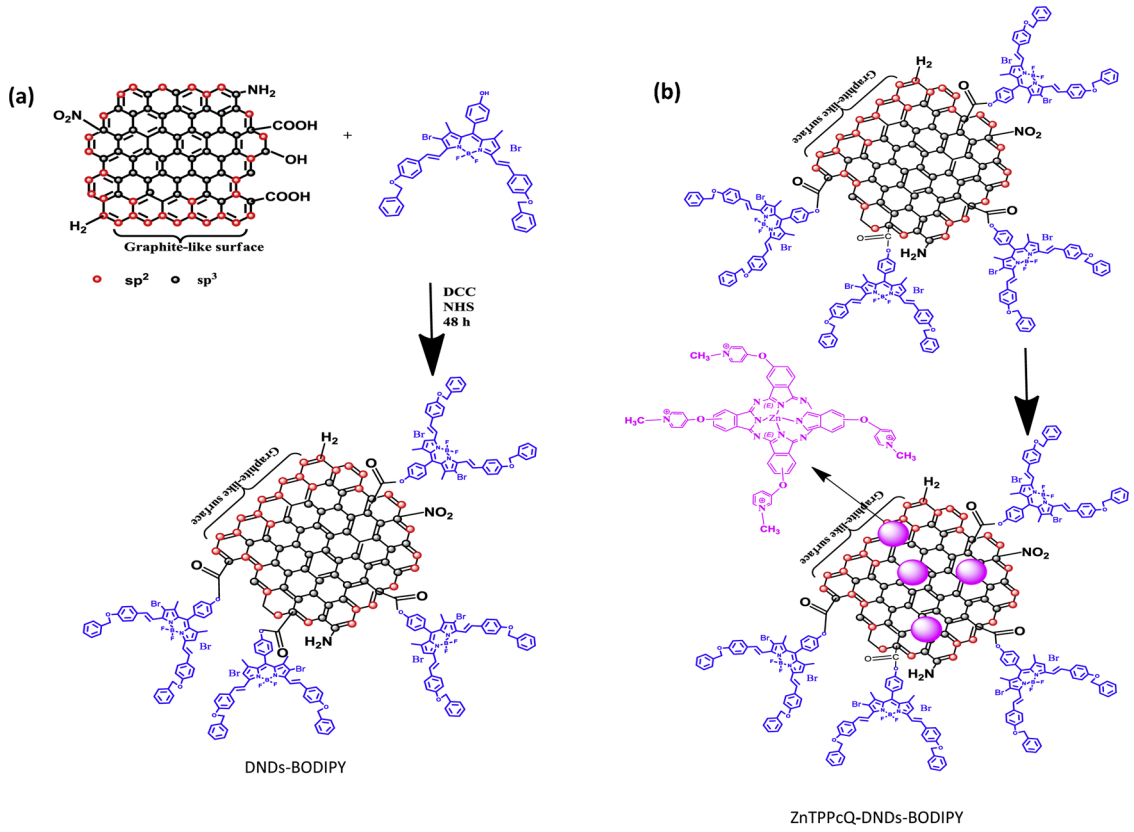

Scheme 1. (a) The ester covalent linkage of BODIPY and detonated nanodiamonds (DNDs) resulting in DNDs-BODIPY nanoconjugate systems. (b) $\pi - \pi$ interaction between ZnTPPcQ and DNDs-BODIPY to form ZnTPPcQ-DNDs-BODIPY.

have negative net charge [21]. To the best our knowledge, BODIPY/MPc decorated DNDs are not known and are thus reported for the first time in this work.

The composites were constructed as follows: DNDs contained carboxylic functional groups which assisted in the covalent linking to the hydroxyl moiety of the BODIPY dye to form DNDs-BODIPY, Scheme 1A. The presence of sp^2 hybridisation in DNDs allows for ππ interactions with other π containing molecules such as MPcs, hence the reported 2,9,16,23-tetrakis[4-(*N*-methylpyridyloxy)]-phthalocyanine (ZnTPPcQ) [3,22] was then adsorbed onto DNDs-BODIPY via π–π stacking interaction to form nanoassembly of ZnTPPcQ-DNDs-BODIPY, Scheme 1b. ZnTPPcQ was also adsorbed onto the DNDs in the absence of the BODIPY. π–π stacking is also possible for DNDs-BODIPY in addition to the covalent bond. We report on the photophysical properties and PDT activities of the nanocomposites.

2. Experimental

2.1. Materials

Detonated nanodiamonds (DNDs), 1, 3-diphenylisobenzofuran (DPBF), trifluoro acetic acid (TFA), *N*-hydroxysuccinimide (NHS), Zn phthalocyanine (ZnPc), and anthracene-9,10-bis-methylmalonate (ADMA) were obtained from Sigma–Aldrich. *N,N′*-dicyclohexylcarbodiimide (DCC) was purchased from Merck. Dimethyl sulfoxide (DMSO), methanol, and ethanol were purchased from SAARCHEM. All aqueous solutions were prepared using from Milli–Q Water System (Millipore Corp, Bedford, MA, USA). All other reagents and solvents were obtained from commercial suppliers and were of analytical grade and used as received. MCF-7 breast cancer cells were obtained from Cellonex. Dulbecco's phosphate-buffered saline (DPBS) and Dulbecco's modified Eagle's medium (DMEM) were obtained from Lonza, 10% (v/v) heat-inactivated fetal calf serum (FCS), 100 mg/mL-penicillin–100 unit/mL-streptomycin–amphotericin B mixture) were obtained from Biowest®. The syntheses of 3,5-di-*p*-benzyloxystyryl BODIPY [15], 2,9,16,23-tetrakis[4-(*N*-methylpyridyloxy)]-phthalocyanine (ZnTPPcQ) [3,22] and AlPcSmix (containing a mixture of differently sulfonated Pcs, used as a standard for singlet oxygen determinations in water) [23] have been reported before. Ludox solution obtained from Sigma Aldrich was used as a standard in order to determine fluorescence lifetimes from time-correlated single photon counting (TCSPC) following methods reported in literature [24].

Equipment items employed in this work are located in the Supporting Information.

2.2. Synthesis

2.2.1. Linkage of hydroxyphenyl-BODIPY to DNDs (Scheme 1a)

Linkage of nanoparticles to BODIPY dye was conducted following previous methods with slight modification [14,25]. Briefly, DNDs (20 mg) were dissolved in DMSO (3 ml). Then DCC (0.02 g, 0.098 mmol) and NHS (0.015 g, 0.13 mmol) were added and the resulting solution was stirred for 48 h in order to activate the carboxylic groups of the DNDs, following which the BODIPY dye (0.008 g, 0.01 mmol) was added and the mixture further stirred for 48 h. The resulting conjugate (DNDs-BODIPY) was precipitated out from solution with trifluoro acetic acid (TFA) and ice. The precipitate was washed several times with water, centrifuged, and then dried in the fume hood to obtain the DNDs-BODIPY.

2.2.2. Construction of ZnTPPcQ-DNDs-BODIPY and ZnTPPcQ-DNDs nanoassembly (Scheme 1b)

Nanoassemblies shown in Scheme 1b were prepared following previous methods with alterations [14]. Briefly, the ZnTPPcQ (0.01 g;

0.01 mmol) was adsorbed onto DNDs-BODIPY (10 mg) or DNDs (10 mg) through π-π stacking in 3 mL DMSO. The resulting mixture was ultrasonicated for 4 h, followed by stirring for 96 h. The resulting conjugates were precipitated out of solution with ethanol to ensure that uncomplexed DNDs-BODIPY, DNDs and Pc were eliminated. The solid products were then dried under vacuum and are represented as ZnTPPcQ-DNDs-BODIPY and ZnTPPcQ-DNDs.

2.3. Physicochemical parameters

Fluorescence (Φ_F) and triplet (Φ_T) quantum yields were determined in DMSO using comparative methods described before [26–28]. Unsubstituted ZnPc in DMSO was used as a standard with $\Phi_F = 0.20$ [27] and $\Phi_T = 0.65$ [29]. Singlet oxygen quantum yield (Φ_Δ) values were determined under ambient conditions using DPBF as a singlet oxygen quencher in DMSO (and ADMA in water containing 1% DMSO for all samples) using equations described previously [30,31]. ZnPc in DMSO was used as a standard ($\Phi_\Delta = 0.67$) [30]. AlPcSmix was employed as a standard in aqueous media ($\Phi_\Delta = 0.42$) [28]. The absorbances of DPBF or ADMA were spectroscopically monitored at 417 nm or 380 nm, respectively, at predetermined time intervals.

2.4. In vitro cell studies

In vitro dark cytotoxicity and photodynamic therapy (PDT) were carried out following previous reports [32,33]. MCF-7 cancer cell lines were cultivated as a monolayer in T75 cm^2 culture flasks in DMEM supplemented with 10% heat-inactivated fetal calf serum (FCS), 1% amphotericin B and 1% penicillin-streptomycin mixture. Cells were incubated at 37 °C in a 5% CO_2 humidified incubator.

After reaching 70–80% confluence, cells were detached from the flask using trypsin. The activity of trypsin was quenched by adding fresh supplemented DMEM, and the cells were centrifuged for 2 min at 2000 rpm. Viable cells were manually counted with the Neubauer hemocytometer cell counter, using the trypan blue exclusion test of viability. A concentration of 10^4 cells was seeded and incubated with different concentrations (5, 10, 20, 40 and 50 μg/ml) of DNDs, BODIPY, ZnTPPcQ, DNDs-BODIPY, ZnTPPcQ-DNDs and ZnTPPcQ-DNDs-BODIPY for dark toxicity and PDT studies. DNDs, ZnTPPcQ, ZnTPPcQ-DNDs and ZnTPPcQ-DNDs-BODIPY are soluble in water while DNDs-BODIPY is partly soluble. In order to have the same environment for cell studies, stock solutions of the complexes were prepared in DMSO and made up with culture medium. The total amount of DMSO was 1%. The cells were incubated for 24 h with 1% (v/v) of DMSO in supplemented media in order to assess the effects of DMSO. The surviving cells were subsequently quantified using the WST-1 cell proliferation assay 24 h after the treatment.

2.4.1. Dark cytotoxicity

Cells were incubated for 24 h with different concentrations of photosentisisers: DNDs, BODIPY, ZnTPPcQ, DNDs-BODIPY, ZnTPPcQ-DNDs and ZnTPPcQ-DNDs-BODIPY as stated above. The media containing the photosensitisers was removed and cells were washed with DPBS. Fresh media was added, and cells were further incubated for 24 h.

The tetrazolium compound reagent (WST-1, Roche) was used for the quantification of cell proliferation and cell viability. It is a colorimetric assay and based on the cleavage of the tetrazolium salt (WST-1) by mitochondrial dehydrogenases in proliferating cells [34]. The WST-1 assay was used as per manufacturer's instructions (Roche) using a Synergy 2 multi-mode microplate reader (BioTek®) at a wavelength of 450 nm.

The percent cell viability was determined using Eq. (1):

$$\%\ cell\ viability = \frac{Absorbance\ sample\ at\ 450\,nm}{Absorbance\ control\ at\ 450\,nm} \times 100 \quad (1)$$

2.4.2. Photodynamic therapy (PDT) studies

Photo irradiation for PDT studies were done using a General Electric Quartz line projector lamp (300 W). A 600 nm glass cut off filter (Schott) and a water filter were used to filter off ultraviolet and infrared radiations, respectively. An interference filter (Intor, 670 nm with a bandwidth of 40 nm) was additionally placed in the light path before the sample. Light intensities were measured with a POWER MAX5100 (Molelectron detector incorporated) power meter and were found to be 14.2×10^{18} photons s^{-1} cm^{-2} for PDT studies. The light source was linked to an illumination kit, with a capacity to hold a 127.76 × 85.48 mm 96 well tissue culture plate for *in vitro* PDT studies.

Cells were incubated for 24 h with different concentrations of BODIPY, ZnTPPcQ, DNDs-BODIPY, ZnTPPcQ-DNDs and ZnTPPcQ-DNDs-BODIPY as stated above. Wells were washed twice with DPBS and the culture media was replaced with the fresh media (with no phenol red). The wells containing cells were illuminated. After irradiation, the culture media (without phenol red) was replaced with the fresh media containing phenol red. Cells were incubated for 24 h at 37 °C in 5% CO_2, cellular viability was expressed in percentage.

2.4.3. Statistical analysis

The data obtained from the three independent (n = 3) triplicate experiments were analysed with a 3-way factorial ANOVA (analysis of variance) to determine the statistical differences between the *in vitro* cytotoxicity and photodynamic effect of the photosensitisers on MCF-7 cancer cells. A p-value of < 0.01 was considered significant.

3. Results and discussion

3.1. Synthesis and characterisation

DNDs-BODIPY nanoassembly (Scheme 1a) was obtained through ester bond formation between the carboxyl moiety of the DNDs and the hydroxyl of the BODIPY. Ester linkage between DNDs and BODIPY was confirmed using FTIR (Fig. 1). The covalent linkage between DNDs and BODIPY was confirmed by an emergence of an ester bond peak around 1627 cm^{-1} (Fig. 1(c)). The FT-IR spectrum of the BODIPY in Fig. 1(a) confirmed the presence of ROH and B–N at 2897 and 1440 cm^{-1}. While COOH, C═O and C—H peaks at 3384, 1624 and 625 cm^{-1}, respectively, Fig. 1(b), were observed for DNDs. Slight shifts of of the C═O, B—N, ROH and COOH peaks to 1562, 1444, 2922 and 3328 cm^{-1} were observed upon linkage of the BODIPY to the DNDs. Shifts in the IR bands confirm structural change [35].

TEM images showed monodispersed DNDs when alone (Fig. 2(a)) and clusters for nanoconjugates, Fig. 2 (b,c). The size of DNDs alone as determined by TEM was 2.1 nm. There was an increase in size upon conjugation to 4.1 and 6.5 nm, for DNDs-BODIPY and ZnTPPcQ-DNDs-BODIPY, respectively (shown as examples in Fig. 2). Such increases in size upon conjugation of BODIPY or Pcs to other nanoparticles such as GQDs have been reported to be due to aggregation [14,36,37]. Dynamic light scattering (DLS) analysis, Fig. 3, revealed average hydrodynamic sizes of 2.3 nm, 4.5 nm, and 7.5 nm for DNDs, DNDs-BODIPY and ZnTPPcQ-DNDs-BODIPY, Table 1. Sizes determined by DLS have been reported to be larger than those determined by other methods since DLS sizes tend to be skewed toward larger particles [38], hence DLS sizes are larger than those obtained with TEM in this work.

Zeta potential is a measure of charges carried by particles suspended in a liquid (mostly water). It is an important parameter in the fabrication of supramolecular structures as a high zeta potential confers colloidal stability. Therefore, zeta potential values of nanoconjugated assembles intended for biomedical applications gives an indication of aggregation tendencies in aqueous media [39]. Previous studies have shown that temperature, pH and sample concentration are amongst other factors that can influence the zeta potential [40]. In this study, different temperatures (11, 22, 37, 60 and 80 °C), pHs (2, 4, 7, 10 and 13) and concentrations (5, 10, 20, 40 and 50 μg/ml (m/v)) were

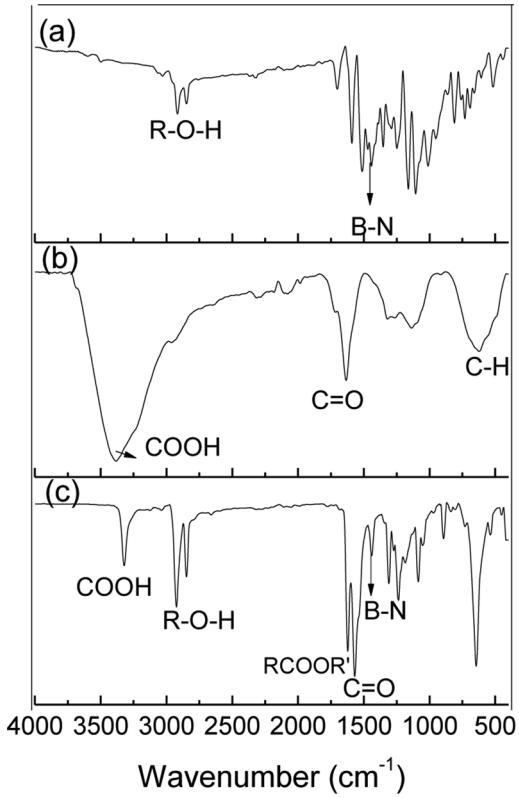

Fig. 1. FTIR spectra of (a) BODIPY, (b) DNDs, and (c) DNDs-BODIPY showing formation of ester bond.

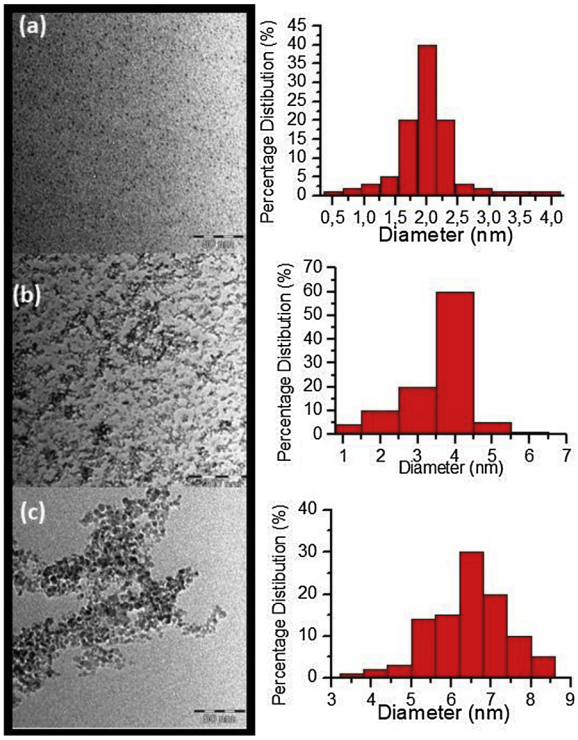

Fig. 2. TEM images of (a) DNDs, (b) DNDs-BODIPY and (c) ZnTPPcQ-DNDs-BODIPY showing morphology and particles size distribution of constructed nanoassemblies.

employed.

In this work, zeta potential was carried out in water instead of cultured medium because previous studies on nanoparticles have shown that cultured media contain albumin protein which is negatively charged at neutral pH and can adsorb to the surface of the nanoparticle to influence their zeta potential [41,42].

Fig. 4(a) illustrates the zeta potential measurement as a function of pH for DNDs nanoparticles with or without BODIPY and/or ZnTPPcQ conjugation. Zeta potential values of DNDs increased (became more positive or more negative) upon conjugation (DNDs-BODIPY, ZnTPPcQ-DNDs and ZnTPPcQ-DNDs-BODIPY) for pH = 2, 4 and 7. Similar increases in zeta potential upon functionalisation of the NDs to doxorubicin (DOX) and TAT (HIV trans-activator of transcription protein) have been previously reported [43]. High zeta potential values, irrespective of charge, infer stability [44]. High zeta potential values following hybrid formation points to improvement in the dispensability of the resulting supramolecular structures, signifying high colloidal stability. When the zeta potential is small, attractive forces may exceed this repulsion, resulting in aggregation [45]. Thus, Fig. 4a shows higher stability for ZnTPPcQ-DNDs-BODIPY when compared to DNDs-BODIPY, ZnTPPcQ-DNDs and DNDs alone at pHs 2, 4 and 7.

To find a suitable concentration of the drug for electrosteric stabilisation of the colloids, different concentrations of ZnTPPcQ-DNDs-BODIPY were investigated in aqueous medium prior to *in vitro* cell studies. Suspensions that have a measured zeta potential above 30 mV or below −30 mV are considered stable because these particles will presumably maintain their repulsive forces while dispersed [46,47].

Fig. 4(b) demonstraes general stability of ZnTPPcQ-DNDs-BODIPY (-51, -44, -39, -32 and 183 mV) at various drug concentrations (5, 10, 20, 40 and 50 μg/mL), respectively, in aqueous media. ZnTPPcQ-DNDs-BODIPY showed the most stability at a high concentration of 50 μg/mL when both pH (7) and temperature (37 °C) remained constant. Therefore, high concentrations of the nanoconjugate resulted in high zeta potential value. Similar increases in the zeta potential with increasing concentration to that obtained in Fig. 4(b), have been previously reported as an indication of neutralisation of surface charges in a solution [40,44].

Fig. 4(c) shows zeta-potential measurements as a function of the temperature of the solution at approximately 11, 22, 37, 60 and 80 °C for 50 μg/mL concentrated solution at pH 7. The behaviour of constructed ZnTPPcQ-DNDs-BODIPY nanoconjugate system was investigated in order to understand the effect of temperature on the nanohybrid. It is observed that zeta potential increases as the temperature is increased indicating stability of the compound. This behaviour is consistent with experimental results from previous studies [40]. Therefore, an increase in body temperature will not compromise the stability of the drug but rather improve it.

The zeta potentials of the nanoassemblies of DNDs-BODIPY, ZnTPPcQ-DNDs and ZnTPPcQ-DNDs-BODIPY were determined at constant temperature (27 °C), concentration (10 $\mu g.ml^{-1}$) and pH = 7 and showed zeta potentials of -48.6, -48.9 and -58.3 mV, respectively were obtained, Table 1. Zeta potentials of DNDs, ZnTPPcQ and BODIPY alone were 43.0, 15.0 to 64.7 mV, respectively, Table 1. Thus, from the zeta potential values listed in Table 1, DNDs, BODIPY, DNDs-BODIPY, ZnTPPcQ-DNDs and ZnTPPcQ-DNDs-BODIPY with values > ± 30 mV may be considered to be stable, while ZnTPPcQ is unstable. Surprisingly, DNDs showed positive surface charge despite the predominant carboxylic acid groups on the ND surface shown in FT-IR. Similar observations have been attributed to carbon basicity (due to oxygen defects) [46].

Raman spectra were used to determine the quality of the constructed DNDs nanoassemblies. The disorder (D) sp^3 defects and graphitic (G) sp^2 peaks from in plane vibrations were observed at 1369 and 1585 cm^{-1}, respectively (Fig. 5(a)) for DNDs alone. The D bands of the DNDs-BODIPY (Fig. 5(b)) and ZnTPPcQ-DNDs-BODIPY (Fig. 5(c)) shift to lower wavenumbers compared to DNDs alone. Shifts in the Raman frequencies are often indicative of strong π-electron interactions in hybrid materials [48]. The G bands for DNDs, DNDs-BODIPY and ZnTPPcQ-DNDs-BODIPY did not shift as well as the D band for

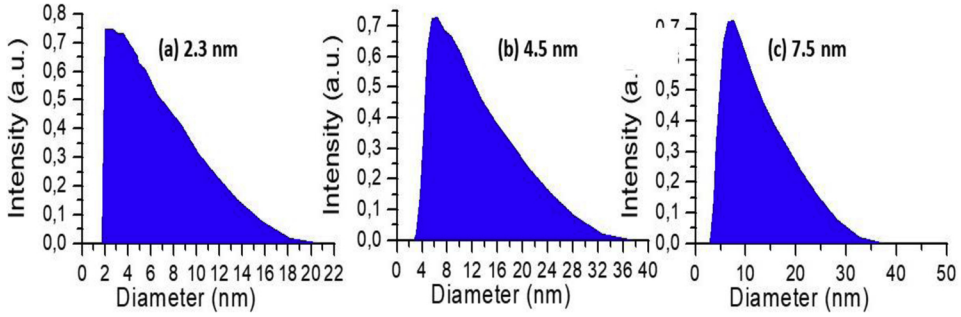

Fig. 3. DLS plots of (a) DNDs, (b) DNDs-BODIPY and (c) ZnTPPcQ-DNDs-BODIPY.

ZnTPPcQ-DNDs.

The I_D: I_G (sp^3:sp^2) ratio is generally considered as a quality parameter to determine the extent of functionalisation of the carbon nanomaterials. This is because the intensity of the G-band is not affected by defects, whereas the D-band is enhanced by the presence of sp^3 defects in the sp^2 lattice. Conjugation to form ZnTPPcQ-DNDs (0.15), DNDs-BODIPY (0.25) and ZnTPPcQ-DNDs-BODIPY (0.33) resulted in increased DNDs (0.01) defects as judged by the increase in I_D:I_G ratio, Table 1. This increase in disorder could have been due to BODIPY and ZnTPPcQ, causing more stress/strain onto the nanoparticle. The increase or decrease in I_D:I_G ratio of GQDs has been previously reported to be due to size-dependent edge-state variation of GQDs [48]. A similar increase in the I_D:I_G ratio has been reported for GQDs nanoconjugates of BODIPY and phthalocyanines [14]. This indicates that doping DNDs with BODIPY and Pc loading increased the strain/stress and defects.

Theromogravimetric analyses of DNDs, BODIPY, ZnTPPcQ, DNDs-BODIPY and ZnTPPcQ-DNDs-BODIPY were conducted in the temperature range of 50–1000 °C in air and the results are presented in Fig. 6. In comparison with DNDs (97%), the TGA curves for DNDs-BODIPY, ZnTPPcQ-DNDs and ZnTPPcQ-DNDs-BODIPY revealed a decreased weight loss of 75, 94 and 37%, respectively, which was correlated to the thermal decomposition of the grafted BODIPY and ZnTPPcQ. ZnTPPcQ-DNDs-BODIPY showed less weight loss compared to DNDs-BODIPY and ZnTPPcQ-DNDs. A possible explanation for this might be due to the presence of nitrogen in both the BODIPY and ZnTPPcQ which forms a heat resistant protective network, thus somehow retarding the weight loss of ZnTPPcQ-DNDs-BODIPY. Similar formation of nitrogen protective network due to temperature increase in TAT-ND-DOX has been reported to yield less weight loss [43]. Hence, functionalisation of DNDs improved the thermal stability of constructed conjugates. Mass loading ratios were calculated from TGA, using DNDs decomposition as a point of reference following a previously reported method [49]. The respective masses of ZnTPPcQ and/or BODIPY loaded onto DNDs are as follows: ZnTPPcQ-DNDs, BODIPY-DNDs and ZnTPPcQ-DNDs-BODIPY 30.89, 282.34 and 333.63 μg Pc per mg DNDs, respectively, as shown in Table 1.

Fig. 7(a) and (b) shows UV–vis absorption spectra of DNDs, Pcs, BODIPY and their conjugates, separately dispersed in DMSO and water, respectively. The broad absorption band of DNDs in both solvents, is associated with absorption peaks from π–π* transition of aromatic sp^2 domains in the material [50]. The ground state absorption spectra of Pcs are dominated by two major absorption bands in the visible or near infrared (IR) (670–1000 nm) and the UV (325–370 nm) regions corresponding to the Q and the B bands, respectively [3]. Absorption spectrum for ZnTPPcQ alone (Fig. 7(a)) showed a narrow Q band at 680 nm (Table 1) in DMSO typical of monomeric MPcs [51]. The absorption maximum for BODIPY at 649 nm has been previously reported [15]. There was a red shift (and broadening) in the spectrum of BODIPY upon conjugation to DNDs. Similar red shifts and peak broadening upon conjugation of BODIPY to nanoparticles has been previously reported [52]. In water, extensive aggregation occurred as judged by peak broadening shown in Fig. 7(b) of the dyes, typical of Pcs in aqueous media [51].

3.2. Photophysicochemical properties

Decreases in fluorescence quantum yields (Φ_F) and lifetimes (τ_F) of photosensitisers (BODIPY and ZnTPPcQ) were observed in the presence of DNDs for ZnTPPcQ-DNDs and DNDs-BODIPY, respectively. For ZnTPPcQ-DNDs-BODIPY the Φ_F and τ_F values are less than that for ZnTPPcQ and BODIPY alone. It is important to note that excitation wavelength used for Φ_F and τ_F value determinations at 649 nm, and 670 nm, respectively will excite both the BODIPY and Pcs, hence the Φ_F and τ_F values are influenced by both photosensitisers. Fluorescence quantum yield and lifetime have direct relationship, hence they both decreased. BODIPY alone showed high fluorescence quantum yields, typical of BODIPYs [53].

The triplet quantum yield of ZnTPPcQ (Φ_T = 0.73) increased

Table 1
Parameters for BODIPY, ZnTPPcQ, DNDs-BODIPY, ZnTPPcQ-DNDs and ZnTPPcQ-DNDs-BODIPY in DMSO (unless otherwise stated).

Sample	λ (nm)	DLS size (nm)	Mass Ratio Loading (μg Pc/mg QDs)	Zeta potential ξ (mV)[a]	Raman spectra I_D/I_G ratio	Φ_F	τ_F (ns)[b]	Φ_T	τ_T (μs)	Φ_Δ[f]
DNDs	–	2.3		43.0	0.01	–	–	–	–	–
BODIPY	649	1.5		64.7	–	0.53[c]	3.87[c]	-[d]	-[d]	0.32 (0.24)
ZnTPPcQ	680	0.7		15.0	–	0.18	2.74[e]	0.73 [e]	326[e]	0.41[d](0.03)
ZnTPPcQ-DNDs	679	3.9	30.89	−48.9	0.15	0.15	2.69	0.75	301.5	0.62(0.05)
DNDs-BODIPY	675	4.5	282.34	−48.6	0.25	0.11	2.64	-[d]	-[d]	0.68(0.36)
ZnTPPcQ-DNDs-BODIPY	683	7.5	333.63	−58.3	0.33	0.10	2.61	0.76	228.9	0.73 (0.50)

[a] temperature (27 °C), concentration (10 μg.ml^{-1}) and pH = 7.
[b] excitation wavelength = **670** nm for BODIPY and Pcs.
[c] Values from reference **15**.
[d] No signal.
[e] Values from reference **37**.
[f] Values in brackets in water (containing 1% DMSO).

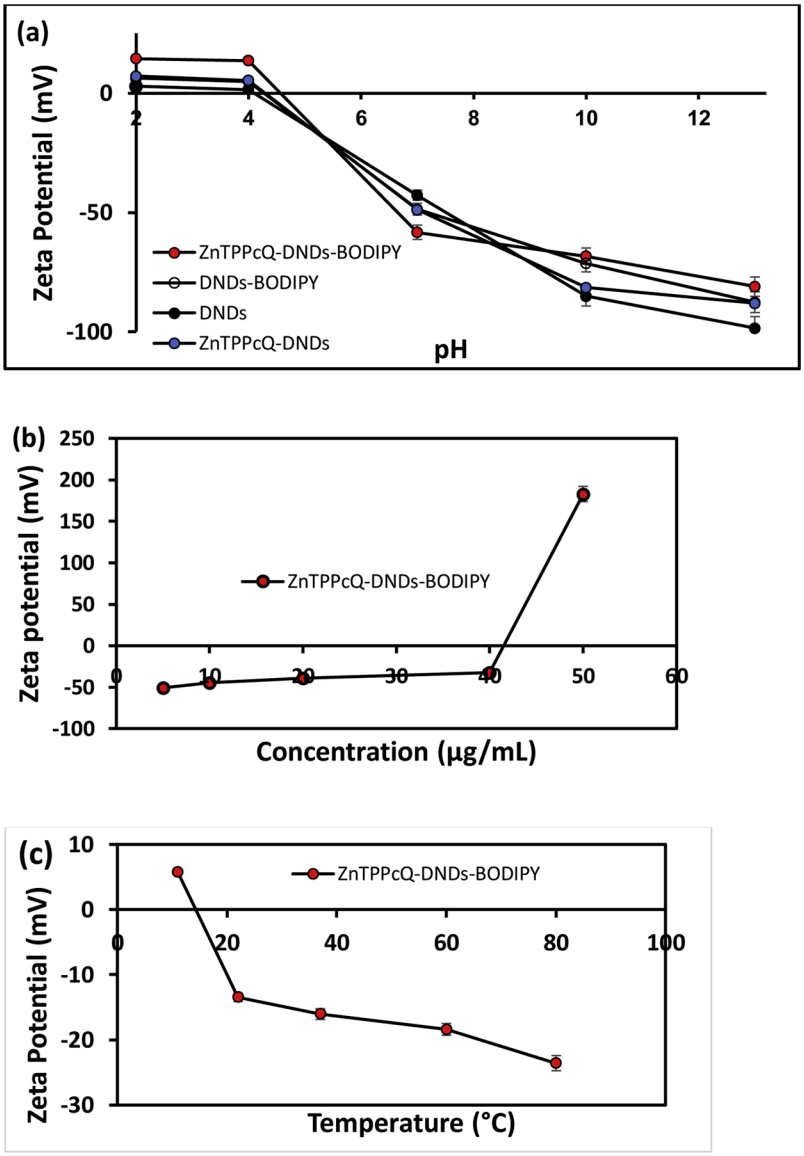

Fig. 4. Zeta potential plots for (a) DNDs and conjugates as function of pH when concentration (50 µg/mL) and temperaturel (27 °C) are kept constant; (b) ZnTPPcQ-DNDs-BODIPY at different concentrations, but at a constant temperature of (37 °C) and neutral pH (7), and (c) ZnTPPcQ-DNDs-BODIPY at a constant concentration (50 µg/mL) and neutral pH (7) as the temperature of the aquesous medium changes.

slightly in the presence of DNDs for ZnTPPcQ-DNDs (Φ_T = 0.75) and ZnTPPcQ-DNDs-BODIPY (Φ_T = 0.76). Φ_T increased where there was a decrease in Φ_F since the two are competing processes. The Φ_T values for BODIPY and DNDs-BODIPY could not be determined due to lack of a signal. The triplet lifetimes decreased with increase in triplet quantum yields as expected [54].

Singlet quantum yields are an indication of the energy transfer from triplet excited state of a photosensitiser to ground state molecular oxygen. Therefore, singlet oxygen generation depends on triplet quantum yield and triplet lifetime of a photosentisiser. Singlet oxygen quantum yield (Φ_Δ) values were determined under ambient conditions using DPBF and ADMA as singlet oxygen scavengers in DMSO and water, respectively, Fig. 8. Gradual decrease in absorption bands of both DPBF and ADMA with increase in irradiation time was observed while the Q band of the Pc remained the same, indicating photostability of the Pc. The Φ_Δ values in DMSO were calculated to be 0.32, 0.41, 0.62, 0.68, and 0.73 for BODIPY, ZnTPPcQ, ZnTPPcQ-DNDs, DNDs-BODIPY and ZnTPPcQ-DNDs-BODIPY, respectively. For ZnTPPcQ-DNDs-BODIPY, both BODIPY and Pc are excited. The increase in the Φ_Δ values for ZnTPPcQ-DNDs and ZnTPPcQ-DNDs-BODIPY corresponds to the increase in the triplet quantum yields since singlet oxygen is generated from the triplet state. The increase in Φ_Δ for DNDs-BODIPY compared to BODIPY corresponds to the decrease in fluorescence quantum yields. The increase in Φ_Δ shows that BODIPYs are more viable photosensizers in the presence of DNDs. A dramatic drop in the Φ_Δ values in water was observed. This could be due to the fact that oxygen has higher solubility in many organic solvents compared to water [55], which could be responsible for the low singlet oxygen generation in water.

3.3. MCF-7 breast cancer cell studies

3.3.1. In vitro dark cytotoxicity

Dark cytotoxicity studies of DNDs, BODIPY, ZnTPPcQ, DNDs-BODIPY, ZnTPPcQ-DNDs and ZnTPPcQ-DNDs-BODIPY were performed *in vitro* on MCF-7 cancer cells by quantification of surviving cells using the WST-1 cell proliferation assay 24 h after the treatment with 5–50 µg/ml concentrations of the complexes and conjugates (Fig. 9, Fig. S1, in Supporting Information). The control cells showed 99.5 ± 1% viable cells, suggesting that 1% (v/v) DMSO in supplemented media

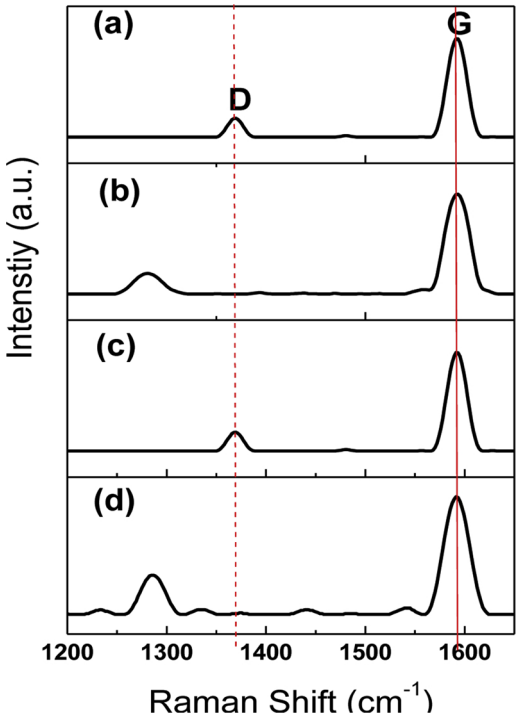

Fig. 5. Raman spectra of (a) DNDs, (b) DNDs-BODIPY (c) ZnTPPcQ-DNDs and (d) ZnTPPcQ-DNDs-BODIPY.

had a negligible effect on the cells (Fig. 9). The dark toxicity in cell culture which was used as the stock solution diluent was found to be similar with what was obtained in supplemented DMEM alone. Photosensitisers showed negligible dark toxicity on MCF-7 with cell viability at the highest tested concentration (50 μg/mL) being as follows: DNDs (98.2 ± 4%), BODIPY (99.4 ± 1%), ZnTPPcQ (99.3 ± 1%), DNDs-BODIPY (100 ± 7%), ZnTPPcQ-DNDs (100 ± 1%) and ZnTPPcQ-DNDs-BODIPY (98.6 ± 3%), Fig. 9(a) and S1a. In general, it was observed that there was no statistically significant difference in the percent viability of the cells as the concentration of the photosensitisers increases. Upon analysis of the triplicate replicate data of each concentration, we observed that there was no statistically significant difference as the p-value was found to be less than 0.05. On average,

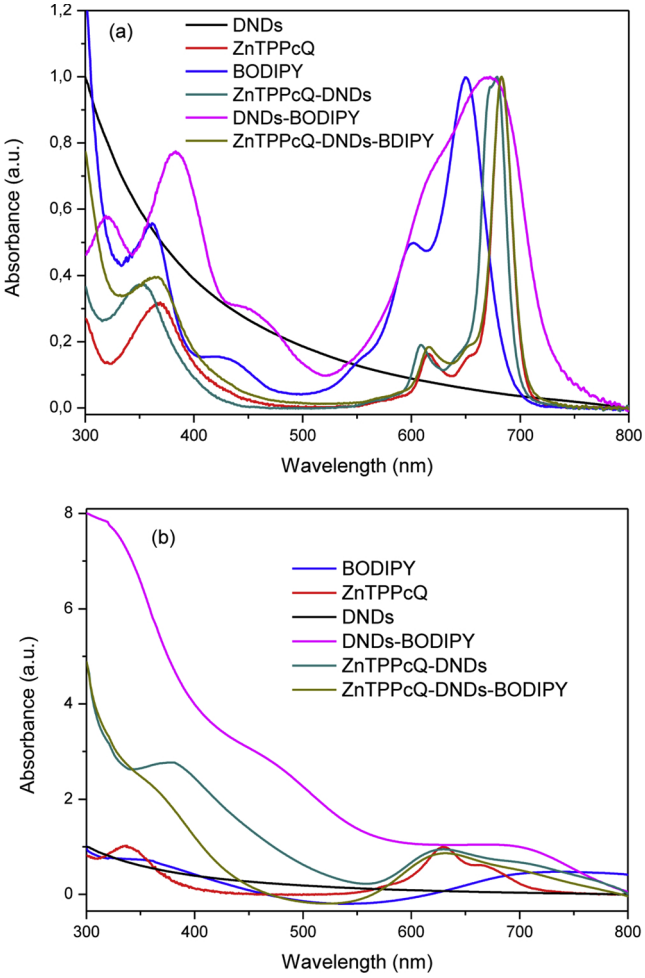

Fig. 7. UV–vis spectra of DNDs, ZnTPPcQ, BODIPY, DNDs-BODIPY, ZnTPPcQ-DND and ZnTPPcQ-DNDs-BODIPY in (a) DMSO and (b) water (containing 1% DMSO) for all samples.

cytotoxicity viability tests of the nanoparticles, dyes and nano-assemblies showed that 97.9 ± 3 of the cells were still viable when compared to those of the control cells. Thus suggesting that there was no

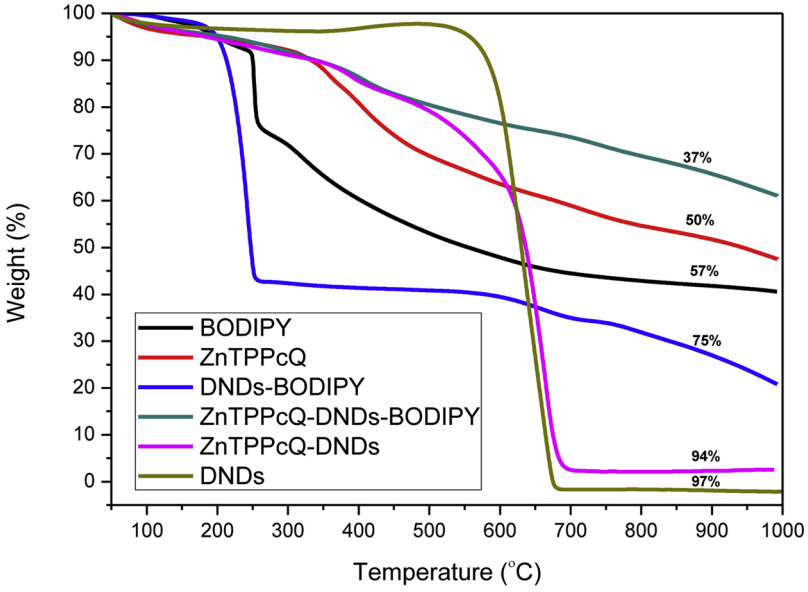

Fig. 6. Thermogravimetric analysis (TGA) curves for samples heated at 20 °C min^{-1} from 50 to 1000 °C in air.

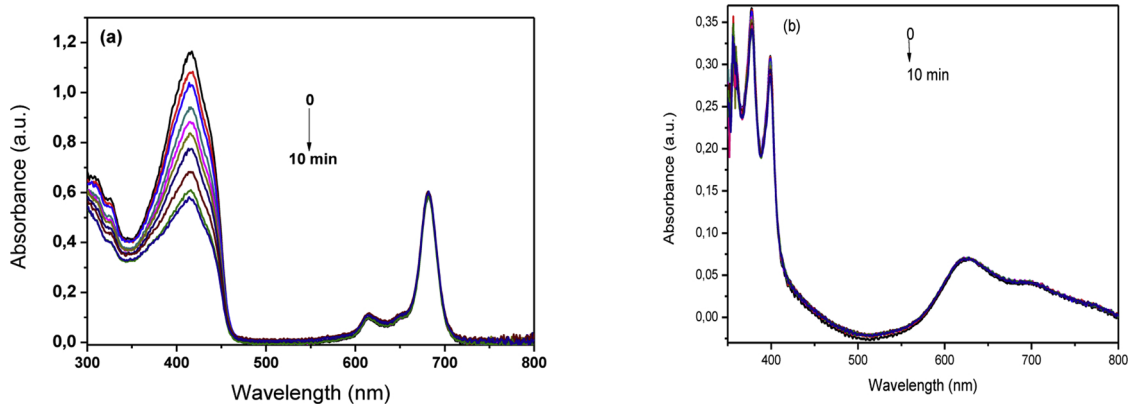

Fig. 8. UV-Vis spectral changes of (a) DPBF in DMSO and (b) ADMA in water using ZnTPPcQ-DNDs-BODIPY as a photosensitizer.

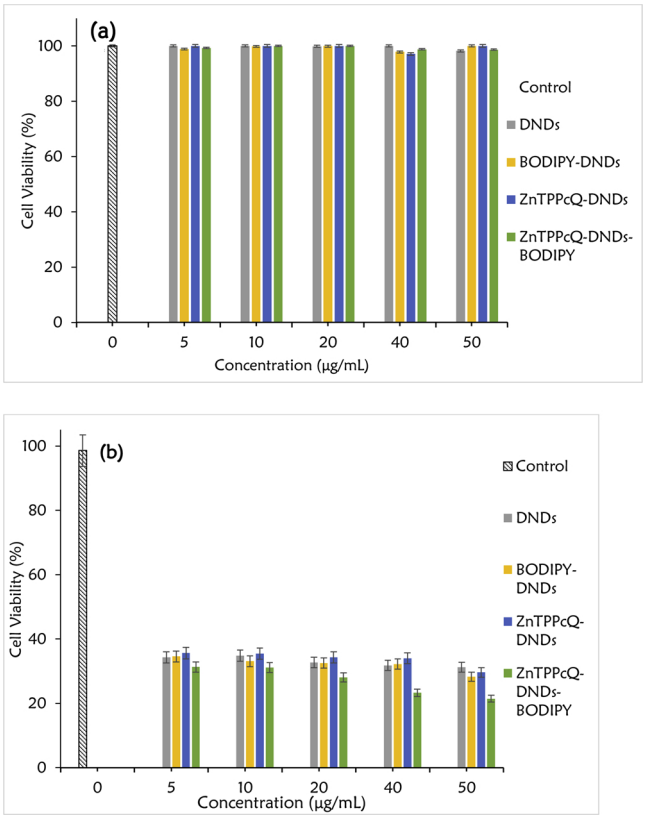

Fig. 9. Dark toxicity on MCF-7 cell lines (a) and PDT (b) plots for DNDs, DNDs-BODIPY, ZnTPPcQ-DNDs and ZnTPPcQ-DNDs-BODIPY. Control (0 mg/mL) conducted in 1% DMSO in growth media. Irradiation time 300 s at 13.5 J/cm^2.

significant difference between the nanoparticles, dyes alone and the constructed nanoassemblies dark cytotoxicity. *In vitro* dark toxicity is not desirable for photosensitisers aimed for use in PDT. Dark cytotoxicity is unwanted in PDT applications because it results in cytocidal activity against both healthy and tumour cells. Thus DND nanoparticles, dyes and nanoassemblies are ideal photosensitisers for PDT.

3.3.2. Photodynamic therapy

The MCF-7 cancer cells were treated with different concentrations (5–50 μg/mL) of DNDs, BODIPY, ZnTPPcQ, DNDs-BODIPY, ZnTPPcQ-DNDs and ZnTPPcQ-DNDs-BODIPY, followed with irradiation of light (13.5 Jcm^{-2}) for 300 s to evaluate the photodynamic therapy activities of the complexes. It should be noted that the effectiveness of a photosensitiser is affected by a number of factors including cell type, cellular uptake, localisation, drug concentration, and irradiation time [32–34]. Only concentration was varied in this work in order to study the effects on the individual components when compared to the composites. The photo-irradiation of MCF-7 cancer cells was done using light from a general electric quartz lamp (following the use of a glass filter) since quartz lamp have been shown to be effective light source in the photo-irradiation of tumour cells [56,57].

Photosensitisers showed significant cytotoxicity on MCF-7 with cell viability at the highest tested concentration (50 μg/mL) of: DNDs (31.2 ± 2%), BODIPY (86.8 ± 2%), ZnTPPcQ (74.7 ± 7%), DNDs-BODIPY (27.7 ± 3%), ZnTPPcQ-DNDs (29.6 ± 2%) and ZnTPPcQ-DNDs-BODIPY (21.4 ± 5%), Fig. 9(b) (and Fig. S1b, supporting information). Thus, ZnTPPcQ-DNDs-BODIPY exhibited the highest phototoxicity towards MCF-7 with only 21 ± 5% cell viability at the highest tested concentration of 50 μg/mL, Fig. 9(b). ZnTPPcQ alone showed low PDT activity with cell viability of ≥75%, while BODIPY alone showed ≥87% at the highest tested concentration, Fig. S1b. For BODIPY (which had a reasonably high singlet oxygen quantum yield in water), the low PDT activity could be due to low permeability into the cell due to the absence of positive charges on the photosensitisers. As stated above, positively charged photosensitisers show higher PDT activity [58,59]. However, despite the positive charge of ZnTPPcQ in ZnTPPcQ-DNDs, the latter showed relatively low PDT activity due to the low singlet oxygen quantum yield properties in water (Table 1). DNDs-BODIPY showed better PDT activity when compared to ZnTPPcQ-DNDs due to the nature of interaction between BODIPY/ZnTPPcQ and the DNDs. Covalently linked nanosystems between Pc and carbon nanostructures have been previously reported to show better properties when compared to non-covalently linked nanosystems [60]. This could be attributed to phase separation between non-covalently linked nanosystems due to the absence of a bond between DNDs and ZnTPPcQ. The higher PDT activity of ZnTPPcQ-DNDs-BODIPY could arise from synergistic effects related to the positively charged sites from the ZnPc complex, BODIPY and DNDs leading to greater spread of singlet oxygen within the cell. The general enhancement in PDT activity of the quaternary complexes could be attributed to introduction of positively charged site which specifically bind to cancer cells and increases cell permeability. The marked increase in PDT activity with increased concentration indicating probable increase in the cellular uptake of complexes as concentration rises. Upon analysis of the triplicate replicate data of each concentration, we observed that there was statistically significant difference as the p-value was found to be less than 0.01.

4. Conclusion

ZnTPPcQ and BODIPY were assembled onto DNDs to form ZnTPPcQ-DNDs, DNDs-BODIPY and ZnTPPcQ-DNDs-BODIPY. A combination of ZnTPPcQ, BODIPY and DNDs showed better

physicochemical properties (triplet and singlet oxygen quantum yields) both in water and DMSO. Colloidal stability of ZnTPPcQ-DNDs-BODIPY was obtained under various temperature, concentration and pH conditions. Zeta potential studies of ZnTPPcQ-DNDs-BODIPY under various temperatures, concentrations and pH conditions, showed the conjugate is more stable at pHs 2, 4 and 7 and at high concentrations (50 μg/mL) and temperatures (80 °C). Thermogravimmetric analysis showed that ZnTPPcQ-DNDs-BODIPY was the most thermally stable. The *in vitro* cytotoxicity test on MCF-7 cancer cells showed that DNDs and respective nanoassemblies; ZnTPPcQ-DNDs, DNDs-BODIPY and ZnTPPcQ-DNDs-BODIPY were relatively not toxic in the absence of light. ZnTPPcQ-DNDs showed cell viability of 30 ± 2%, DNDs-BODIPDY (28 ± 2%) and ZnTPPcQ-DNDs-BODIPY (21 ± 5%). The photodynamic therapy activity was higher for ZnTPPcQ-DNDs-BODIPY, showing that the three component nanoassembly works better than individual components.

Acknowledgements

This work was supported by the Department of Science and Technology (DST) Innovation and National Research Foundation (NRF), South Africa through DST/NRF South African Research Chairs Initiative for Professor of Medicinal Chemistry and Nanotechnology (UID 62620) as well as Rhodes University. Prof Kimura, Kobayashi and E. Osawa from Shinshu University in Japan for the DNDs.

Appendix A. Supplementary data

Supplementary material related to this article can be found, in the online version, at doi:https://doi.org/10.1016/j.pdpdt.2019.03.007.

References

[1] C.G. Claessens, W.J. Blau, M. Cook, M.l. Hanack, R.J.M. Nolte, T. Torres, D. Wöhrle, Phthalocyanines and phthalocyanine analogues: the quest for applicable optical properties, Monatsh. Chem. 132 (2001) 3–11.
[2] S. Luo, E. Zhang, Y. Su, T. Chen, C. Shi, A review of NIR dyes in cancer targeting and imaging, Biomaterials 32 (2011) 7127–7138.
[3] I. Scalise, E.N. Durantini, Synthesis, properties, and photodynamic inactivation of Eschenchia coli using a cationic and a noncharged Zn(II) pyridyloxy phthalocyanine derivative, Bio Inorg. Med. Chem. 13 (2005) 3037–3045.
[4] L.B. Josefsen, R.W. Boyle, Photodynamic therapy and the development of metal-based photosensitisers, Met. Drugs 2008 (2007) Article ID 276109 24 pages.
[5] T.J. Dougherty, C.J. Gomer, B.W. Henderson, G. Jori, D. Kessel, M. Korbelik, J. Moan, Q. Peng, Photodynamic therapy, J. Natl. Cancer Inst. 90 (1998) 889–905.
[6] R. Bonnett, Chemical aspects of photodynamic therapy, Gordon and breach, science publishers, Amsterdam (2000) 305.
[7] E. Ben-Hur, I. Rosenthal, Photosensitized inactivation of Chinese hamster cells by phthalocyanines, Photochem. Photobiol. 42 (1985) 129–133.
[8] G. Mazzone, D.A. Quartarolo, N. Russo, PDT-correlated photophysical properties of thienopyrrole BODIPY derivatives. Theoretical insights, Dyes Pigm. 130 (2016) 9–15.
[9] Z. Wang, X. Hong, S. Zong, C. Tang, Y. Cui, Q. Zheng, BODIPY-doped silica nanoparticles with reduced dye leakage and enhanced singlet oxygen generation, Sci. Rep. 5 (2015) 12602–12612.
[10] A. Kamkaew, S.H. Lim, H.B. Lee, L.V. Kiew, L.Y. Chung, K. Burgess, BODIPY dyes in photodynamic therapy, Chem. Soc. Rev. 42 (2013) 77–88.
[11] S. Osati, H. Ali, E. Johan, V. Lier, Synthesis and spectral properties of phthalocyanine–BODIPY conjugates, Tetrahedron Lett. 56 (2015) 2049–2053.
[12] H. Yanık, M. Göksel, S. Yes-ilot, M. Durmus, Novel phthalocyanine–BODIPY conjugates and their photophysical and photochemical properties, Tetrahedron Lett. 57 (2016) 2922–2926.
[13] C. Gol, M. Malkoc, S. Yesilot, M. Durmus, Novel zinc(II) phthalocyanine conjugates bearing different numbers of BODIPY and iodine groups as substituents on the periphery, Dyes Pigm. 111 (2014) 81–90.
[14] N. Nwahara, R. Nkhahle, B.P. Ngoy, J. Mack, T. Nyokong, Synthesis and Photophysical properties of BODIPY-decorated graphene quantum dots-phthalocyanines conjugates, New J. Chem. 42 (2018) 6051–6061.
[15] B.P. Ngoy, Z. Hlatshwayo, N. Nwaji, G. Fomo, J. Mack, T. Nyokong, Photophysical and optical limiting properties at 532 nm of BODIPY dyes with p -benzyloxystyryl groups at the 3,5-positions, J. Porphyr. Phthalocyanines 22 (2018) 413–422.
[16] Y. Astuti, F.D. Saputra, S. Wuning, Arnelli, G. Bhaduri, Enrichment of nanodiamond surfaces with carboxyl groups for doxorubicin loading and release, IOP Conf. Ser.: Mater. Sci. Eng 172 (2017) 0120668 pages.
[17] O. Shenderova, V. Zhirnov, D. Brenner, Carbon nanostructures, Crit. Rev. Solid State Mater. Sci. 27 (2002) 227–356.
[18] N.R. Greiner, D.S. Phillips, J.D. Johnson, F. Volk, Diamonds in detonation soot, Nature 333 (1988) 440–442.
[19] V.T. Mathias, H.R. Francis, Properties of carbon clusters in TNT detonation products: graphite–diamond transition, J. Appl. Phys. 62 (1987) 1761–1767.
[20] C. Desai, K. Chen, S. Mitra, Aggregation behavior of nanodiamonds and their functionalized analogs in an aqueous environment, Environ. Sci. Process. Impacts 16 (2014) 518–523.
[21] B. Chen, W. Le, Y. Wang, Z. Li, D. Wang, L. Ren, L. Lin, S. Cui, J.J. Hu, Y. Hu, P. Yang, R.C. Ewing, D. Shi, Z. Cui, Targeting negative surface charges of cancer cells by multifunctional nanoprobes, Theranostics 6 (2016) 1887–1898.
[22] A.M.D. Palma, M.G. Alvarez, A.L. Ochoa, M.E. Milanesio, E.N. Duratini, Optimization of cellular uptake of zinc(II) 2,9,16,23-tetrakis[4-(N-methylpyridyloxy)] phthalocyanine for maximal photoinactivation of *Candida albicans*, Fungal Biol. 117 (2013) 744–751.
[23] M. Ambroz, A. Beeby, A.J. McRobert, M.S.C. Simpson, R.K. Svensen, D. Phillips, Preparative, analytical and fluorescence spectroscopic studies of sulphonatedaluminium phthalocyanine photosensitizers, J. Photochem. Photobiol. B, Biol. 1 (1999) 87–95.
[24] C. Tshangana, T. Nyokong, The photophysical properties of multi-functional quantum dots-magnetic nanoparticles–indium octacarboxy phthalocyanine nanocomposite, J. Fluoresc. 25 (2015) 199–210.
[25] A. Fashina, E. Antunes, T. Nyokong, Photophysical behavior of Zn aminophenoxy substituted phthalocyanine conjugates with carboxylic acid-coated silica nanoparticles: Eff ;ect of point of substitution, J. Mol. Struct. 1068 (2014) 245–25.
[26] S. Fery-Forgues, D. Lavabre, Are fluorescence quantum yields so tricky to measure? A demonstration using familiar stationery products, J. Chem. Educ. 76 (1999) 1260–1264.
[27] A. Ogunsipe, J.Y. Chen, T. Nyokong, Photophysical and photochemical studies of zinc (II) phthalocyanine derivatives—effects of substituents and solvents, New J. Chem. 28 (2004) 822–827.
[28] T. Nyokong, E. Antunes, K.M. Science, K.M. Kadish, R.Guilard Smith (Eds.), The Handbook of Porphyrin, 34 World Scientific, Singapore, 2010, pp. 247–34349 7 chap.
[29] T.H. Tran Thi, C. Desforge, C. Thiec, S. Gaspard, Singlet-singlet and triplet-triplet intramolecular transfer processes in a covalently linked porphyrin-phthalocyanine heterodimer, J. Phys. Chem. 93 (1989) 1226–1233.
[30] N.A. Kuznetsova, N.S. Gretsova, O.A. Yuzhakova, V.M. Negrimovskii, O.L. Kaliya, E.A. Luk'yanets, New reagents for determination of the quantum efficiency of singlet oxygen generation in aqueous media, Russ. J. Gen. Chem. 71 (2001) 36–41.
[31] W. Spiller, H. Kliesch, D. Wohrle, S. Hackbarth, B. Roder, G. Schnurpfeil, Singlet oxygen quantum yields of different photo-sensitizers in polar solvents and micellar solutions, J. Porphyr. Phthalocyanines 2 (1998) 2145–2158.
[32] M. Managa, J. Britton, E. Prinsloo, T. Nyokong, Effects of pluronic silica nanoparticles on the photophysical and photodynamic therapy behavior of triphenyl-p-phenoxy benzoic acid metalloporphyrins, J. Coord. Chem. 69 (2016) 3491–3506.
[33] R.O. Ogbodu, J.L. Limson, E. Prinsloo, T. Nyokong, Photophysical properties and photodynamic therapy effect of zinc phthalocyanine-spermine-single walled carbon nanotube conjugate on MCF-7 breast cancer cell line, Synth. Met. 204 (2015) 122–132.
[34] D. Atilla, N. Saydan, M. Durmus, G. Gürek, T. Khanc, A. R¨uck, H. Walt, T. Nyokong, V. Ahsen, Synthesis and photodynamic potential of tetra- and octa-triethyleneoxysulfonyl substituted zinc phthalocyanines, J. Photochem. Photobiol. A: Chem. 186 (2007) 298–307.
[35] B.C. Smith, Infrared Spectra Interpretation: a System Approach, CRC Press, New York, 1998.
[36] O.J. Achadu, I. Uddin, T. Nyokong, Fluorescence behavior of nanoconjugates of graphene quantum dots and zinc phthalocyanines, J. Photochem. Photobiol. A: Chem. 317 (2016) 12–25.
[37] R. Matshitse, K.E. Sekhosana, O.J. Achadu, T. Nyokong, Characterization and physicochemical studies of the conjugates of graphene quantum dots with differently charged zinc phthalocyanine, J. Coord. Chem. 70 (2017) 3308–3324.
[38] T.G.F. Souza, V.S.T. Ciminelli, N.D.S. Mohallem, A comparison of TEM and DLS methods to characterize size distribution of ceramic nanoparticles, J. Phys. Conf. Ser. 733 (2016) 0120395 Pages.
[39] G.W. Lu, P. Gao, Handbook of non-invasive drug delivery systems, Emul. Microemul. Top. Transdermal Drug Delivery (2010) 66–67 Chapter 3.
[40] E. Rosenbrand, I.L. Fabricius, H. Yuan, Thermally induced permeability reduction due to particle migration in sandstone: the effect of temperature on Kaolinite mobilisation and aggregation, Proceedings: Thirty-Seventh Workshop on Geothermal Reservoir Engineering, (2012) SGP-TR-194 9 Pages.
[41] M. Horie1, K. Fujita, Advances in Molecular Toxicology, Toxicity of Metal Oxides Nanoparticles 5 (2011), pp. 145–178 Chapter 4.
[42] L.K. Limbach, Y. Li, R.N. Grass, T.J. Brunner, M.A. Hintermann, M. Muller, D. G, W.J. Stack, Oxide nanoparticle uptake in human lung fibroblasts: effects of particle size, agglomeration, and diffusion at low concentrations, Environ. Sci. Technol. 39 (2005) 9370–9376.
[43] X. Li, J. Shao, Y. Qin, C. Shao, T. Zheng, L. Ye, TAT-conjugated nanodiamond for the enhanced delivery of doxorubicin, J. Mater. Chem. 21 (2011) 7966–7973.
[44] J. Park, S. Lee, J. Ryu, Y. Hong, T. Kim, A.A. Busnaina, Interfacial and electrokinetic characterization of IPA solutions related to semiconductor wafer drying and cleaning, J. Electrochem. Soc. 153 (2006) G811–G814.
[45] I. Ostolska, M. Wiśniewska, Application of the zeta potential measurements to explanation of colloidal Cr_2O_3 stability mechanism in the presence of the ionic polyamino acids, Colloid Polym. Sci. 292 (2014) 2453.
[46] N. Gibson, O. Shenderova, T.J.M. Luo, S. Moseenkov, V. Bondar, A. Puzyr,

K. Purtov, Z. Fitzgerald, D.W. Brenne, Colloidal stability of modified nanodiamond particles, Diam. Relat. Mater. 18 (2009) 620–626.
[47] H.D. Silva, M.A. Cerqueira, A.A. Vicente, Nanoemulsions for food applications: development and characterization, Food Bioprocess. Technol. 5 (2012) 854–867.
[48] S. Kim, S. Hee, K. Oh, K. Seok, J. Sin, S. Choi, H. Won, C. Sone, Size-dependence of Raman scattering from graphene quantum dots: interplay between shape and thickness, Appl. Phys. Lett. 102 (2013) 0531084 Pages.
[49] S. Thomas, R. Thomas, A.K. Zachariah, R.K. Mishra, Thermal and Rheological Measurement Techniques for Nanomaterials Characterization. Chapter Title: Thermogravimetric Analysis for Characterization of Nanomaterials, Elsevier, Netherlands, 2017, pp. 95–97.
[50] G.S. Yurjev, V.Yu. Dolmatov, J. Superhard, Nanophase and nanocomposite materials II, Mater. Res. Soc. Symp. Proc. 435 (2010) 311–1328.
[51] M.J. Stillman, T. Nyokong, C.C. Leznoff, A.B.P. Lever (Eds.), Phthalocyanines: Properties and Applications, VCH Publishers, New York, 1989Ch 3.
[52] J.H. Gibbs, Z. Zhou, D. Kessel, F.R. Fronczek, S. Pakhomova, M.G. Vicente, Synthesis, spectroscopic, and in vitro investigations of 2,6-diiodo-BODIPYs with PDT and bioimaging applications, J. Photochem. Photobiol. B 145 (2015) 35–47.
[53] R.D. Moriarty, A. Martin, K. Adamson, E. O'Reilly, P. Mollard, R.J. Forster, T.E. Keyes, The application of water soluble, mega-Stokes-shifted BODIPY fluorophores to cell and tissue imaging, J. Microsc. 253 (2014) 204–218.
[54] J.R. Darwent, P. Douglas, A. Harriman, G. Porter, M.C. Richoux, Metal phthalocyanines and porphyrins as photosensitizers for reduction of water to hydrogen, Coord. Chem. Rev. 44 (1982) 83–126.
[55] H. Ramesh, T. Mayr, M. Hobisch, S. Borisov, I. Klimant, U. Krühne, J.M. Woodley, Measurement of oxygen transfer from air into organic solvents, J. Chem. Technol. Biotechnol. 91 (2016) 832–836.
[56] M. Alexiades-Armenakas, Laser-mediated photodynamic therapy, Clin. Dermatol. 24 (2006) 16–25.
[57] R.R. Allison, G.H. Downie, R. Cuenca, X.-H. Hu, C.J. Childs, C.H. Sibata, Photosensitizers in clinical PDT, Photodiagon. Photodyn. Ther. 1 (2004) 27–42.
[58] J.C. Bremner, S.R. Wood, J.K. Bradley, J. Griffiths, G.E. Adams, S.B. Brown, 31P magnetic resonance spectroscopy as a predictor of efficacy in photodynamic therapy using differently charged zinc phthalocyanines, Br. J. Cancer 81 (1991) 616–621.
[59] D. Wöhrle, N. Iskander, G. Graschew, H. Sinn, E.A. Friedrich, W. Maier-Borst, J. Stern, P. Schlag, Synthesis of positively charged phthalocyanines and their activity in the photodynamic therapy of cancer cells, Photochem. Photobiol. 51 (1990) 351–356.
[60] G. Bottari, G. de la Torre, D.M. Guldi, T. Torres, Covalent and noncovalent phthalocyanine-carbon nanostructure systems: synthesis, photoinduced electron transfer, and application to molecular photovoltaics, Chem. Rev. 110 (2010) 6768–6816.